Liquid–liquid phase transition in an ionic model of silica

Renjie Chen, Erik Lascaris, and Jeremy C. Palmer

Liquid–liquid phase transition in an ionic model of silica

Renjie Chen,[1] Erik Lascaris,[2] and Jeremy C. Palmer[1,a)]

[1]*Department of Chemical and Biomolecular Engineering, University of Houston, Houston, Texas 77204, USA*
[2]*Center for Polymer Studies and Department of Physics, Boston University, Boston, Massachusetts 02215, USA*

Recent equation of state calculations [E. Lascaris, Phys. Rev. Lett. **116**, 125701 (2016)] for an ionic model of silica suggest that it undergoes a density-driven, liquid–liquid phase transition (LLPT) similar to the controversial transition hypothesized to exist in deeply supercooled water. Here, we perform extensive free energy calculations to scrutinize the model's low-temperature phase behavior and confirm the existence of a first-order phase transition between two liquids with identical compositions but different densities. The low-density liquid (LDL) exhibits tetrahedral order, which is partially disrupted in the high-density liquid (HDL) by the intrusion of additional particles into the primary neighbor shell. Histogram reweighting methods are applied to locate conditions of HDL–LDL coexistence and the liquid spinodals that bound the two-phase region. Spontaneous liquid–liquid phase separation is also observed directly in large-scale molecular dynamics simulations performed inside the predicted two-phase region. Given its clear LLPT, we anticipate that this model may serve as a paradigm for understanding whether similar transitions occur in water and other tetrahedral liquids. *Published by AIP Publishing.* [http://dx.doi.org/10.1063/1.4984335]

I. INTRODUCTION

Substances that form tetrahedrally coordinated liquid phases (e.g., water, silica, silicon, and carbon) are among the most ubiquitous on earth and play an important role in shaping life on our planet.[1,2] Many of the behaviors exhibited by tetrahedral liquids are anomalous when compared to those of "simple" liquids.[3,4] Water's density anomaly is the canonical example: unlike most liquids which densify as temperature decreases, liquid water expands as it is cooled below 4 °C at atmospheric pressure.[3] The magnitude of water's thermodynamic response functions also increases upon cooling. This anomalous trend begins near water's melting line and becomes significantly more pronounced in the supercooled regime.[3] The isothermal compressibility κ_T and heat capacity C_P of water, for example, increase at an accelerated rate as temperature decreases in the supercooled regime,[5–9] suggesting that these quantities may diverge below the homogeneous nucleation temperature, $T_H \approx 232$ K.[6,10]

Several scenarios have been proposed to explain the unusual thermodynamic behavior of water.[11–15] One thermodynamically consistent theory posits the existence of a liquid–liquid phase transition (LLPT) between a high-density and a low-density liquid (HDL and LDL, respectively) at deeply supercooled conditions. The presence of the liquid-liquid critical point (LLCP) terminating the metastable LLPT would explain the apparent divergent behavior of κ_T and C_P upon cooling. The high-density and low-density glass polymorphs (HDA and LDA) observed in water[16–18] are interpreted in this scenario as structurally arrested forms of the two

hypothesized liquids. Unfortunately, the rapid nucleation of ice near T_H has thus far prevented observation of an LLPT.[3] Recent femtosecond X-ray experiments by Sellberg *et al.*[19] characterized the structure of liquid water below T_H for the first time by probing down to 227 K. Analysis of the data from these experiments, however, suggests that water's LLCP, if it exists, lies below 200 K,[20] indicating that measurements at significantly lower temperatures are needed to test the LLPT hypothesis.

The problem of crystallization can often be avoided in computational studies of supercooled liquids because the characteristic nucleation time is typically long compared to the time scales accessible with simulation.[21–23] Consequently, computer simulation studies have successfully probed the liquid-state properties of water models under deeply supercooled conditions. Although the possibility of an LLPT has been excluded in the coarse-grained mW model of water,[15,24–26] equation of state data for molecular models such as TIP4P/2005,[27,28] TIP5P,[29,30] WAIL,[31] E3B3,[32] and ST2[33–36] are consistent with the existence of a low-temperature LLCP. For most of these models, however, extremely slow structural relaxations frustrate equilibration near the predicted LLCP. The exception is ST2,[33] which exhibits anomalies at higher temperatures than other water models due to its over-structured tetrahedral order.[35] ST2's enhanced tetrahedrality also shifts its LLPT to conditions that are accessible with simulation. Although structural relaxations are still slow under these conditions,[26] advanced free energy techniques have been used to overcome this computational challenge and confirm ST2's LLPT.[37–43]

The LLPT scenario has also been invoked to explain the anomalous behavior of other tetrahedral liquids.

a)Author to whom correspondence should be addressed: jcpalmer@uh.edu

Coarse-grained models of DNA tetramers[44] and tetra-functional patchy particles[45] exhibit water-like anomalies and LLPTs, but their short-range, colloidal interactions are distinct from those of molecular and atomic liquids. It has been proposed that an LLPT occurs in the Stillinger-Weber model of silicon,[46,47] though this interpretation is at odds with recent free energy calculations.[48,49] Hints of a possible LLCP have also been observed in ionic models of silica[50,51] in which Si and O atoms are treated as mobile cations and anions, respectively. These models include the van Beest-Kramer-van Santen (BKS)[52] ionic potential for silica and the model of Woodcock, Angell, and Cheeseman (WAC).[53] Fixed charges are placed on Si and O such that the unit formula of silica SiO_2 is electrically neutral. Tetrahedral networks form in the liquid phases of BKS and WAC, when each Si is tightly coordinated with four oppositely charged nearest O neighbors[54] on average. At low temperatures, each Si also preferentially coordinates with an average of four Si neighbors.[54] Hence Si atoms behave as molecular centers that are networked by Si–O–Si ionic bonds. This structure is analogous to the tetrahedral networks formed in water, in which oxygen centers on neighboring molecules are connected via O–H–O hydrogen bonds. Accordingly, ionic models of silica have been posited to exhibit a similar LLPT involving liquids with different densities but identical compositions.[50,51] Exhaustive equation of state calculations for BKS and WAC, however, find no evidence of an LLPT in the computationally accessible region of their phase diagrams.[55]

Recently it has been shown that an LLPT may be observable in a modified version of the WAC silica model (mWAC), in which the magnitude of the charges placed on Si and O ions is modified to enhance tetrahedral order in the liquid.[56] The initial study of the mWAC model showed that its equation of state and thermodynamic response functions exhibit signatures that are consistent with the presence of an LLCP.[56] Constant pressure molecular dynamics (MD) simulations performed in the predicted two-phase region were also found to exhibit abrupt transitions between a high-density and low-density state,[56] which is reminiscent of the "phase flipping" behavior observed in the vicinity of ST2's LLPT.[39,57]

In light of this strong phenomenological evidence, we perform extensive free energy calculations to rigorously scrutinize the low-temperature phase behavior of the mWAC model. In agreement with the equation of state calculations in Ref. 56, the free energy computed as a function of the system's density below the estimated critical temperature clearly shows two liquid basins separated by a free energy barrier. Using histogram reweighting methods, we identify conditions of approximate L–L coexistence and limits of stability for the HDL and LDL phases. We also perform large-scale MD simulations to show that spontaneous L–L phase separation is observed when systems of more than 100 000 particles are thermally quenched into the two-phase region. Hence our results show that the mWAC model exhibits a density-driven LLPT in the accessible region of its phase diagram. To our knowledge, mWAC is the only other example, besides ST2 water, of an atomistic tetrahedral liquid model in which such a transition has been clearly identified.

II. METHODS

A. Model system

The WAC model[53] treats silica as a 1:2 mixture of Si^{+4} and O^{-2} ions that interact through a non-bonded pair potential

$$U_{WAC}(r_{ij}) = f^2 \frac{1}{4\pi\varepsilon_0} \frac{z_i z_j e^2}{r_{ij}} + A_{ij}\exp(-B_{ij}r_{ij}), \quad (1)$$

where r_{ij} is the ion–ion separation distance. Electrostatic interactions are modeled using the Coulomb potential, where z_i is the charge number ($z_{Si} = +4$, $z_O = -2$), e is the elementary charge, and ε_0 is the permittivity of free space. The ions also experience short-range, excluded volume interactions through the exponential term in Eq. (1), with $A_{SiSi} = 1.917\,991\,469 \times 10^5$ kJ/ mol, $A_{SiO} = 1.751\,644\,217 \times 10^5$ kJ/ mol, $A_{OO} = 1.023\,823\,519 \times 10^5$ kJ/ mol, and $B_{ij} = 34.48$ nm^{-1} for all ion pairs.[55] This parameterization gives Si^{+4} and O^{-2} effective ionic radii of $\sigma_{Si} = 0.1301$ nm and $\sigma_O = 0.1420$ nm, respectively.[55]

Following Ref. 56, we introduce a scaling factor f in the Coulombic term in Eq. (1). This factor was not present in the original model, which is recovered when $f = 1$. Hence the choice of $f \neq 1$ defines a modified WAC model (mWAC), in which electrostatic interactions are scaled. We implement the mWAC potential in our simulations by truncating pair-wise interactions between ions at 1.0 nm and treating long-range contributions to the electrostatic interactions using the particle mesh Ewald method. Parameters for the Ewald summation are chosen to ensure a relative error of less than 10^{-4} in the calculated energy.

B. Free energy methods

We scrutinize the mWAC model's low-temperature phase behavior using the Landau free energy

$$F(\phi) = -k_B T \ln \mathcal{P}(\phi) + \text{const.}, \quad (2)$$

where T is temperature, k_B is Boltzmann's constant, $\mathcal{P}$ is the joint equilibrium probability density function associated with the order parameters $\phi(x^N) = \{\phi_1(x^N), \phi_2(x^N), \ldots, \phi_n(x^N)\}$, and x^N is a generalized coordinate vector specifying the micro-state of the N-particle system. The additive constant in Eq. (2) normalizes $\mathcal{P}$ and sets the choice of standard reference state; it has no bearing on the analysis, however, because phase stability is dictated by the curvature of $F(\phi)$ at constant P and T.

We use the system density ρ as the order parameter for our investigation, which is the natural choice for distinguishing between the HDL and LDL phases involved in the LLPT. The free energy $F(\rho)$ was calculated using stratified umbrella sampling,[58] in which a bias is applied to the system to promote exploration of a targeted region or "window" of the order parameter space. To encourage sampling near a target density ρ^*, a harmonic restraint was applied to the system

$$W(\mathbf{x}^N) = \frac{k}{2}\left[\rho(\mathbf{x}^N) - \rho^*\right]^2, \quad (3)$$

where k is the spring constant. With the choice k = 5 000 $k_B T$ cm^6 g^{-2}, the ρ-space relevant to the LLPT is systematically sampled at each temperature investigated by performing 31 independent umbrella sampling simulations with values of ρ^* ranging from 1.43 to 2.50 g cm^{-3}.

Umbrella sampling was performed by conducting MD simulations in the isothermal–isobaric (NPT) ensemble with GROMACS 4.6.7.[59] A Nosé-Hoover thermostat[60,61] and Parrinello-Rahman barostat[62] were used to maintain the temperature and pressure, respectively. Time constants for the thermostat and barostat were set to 2 ps, and an integration time step of 2 fs was used to propagate the trajectories. The free energy plug-in PLUMED 2.2[63] was used to impose the harmonic umbrella restraint on ρ.

Time series data for ρ and the configurational energy of the system, U_c, were collected during the post-equilibration, production phase of the umbrella sampling simulations. These data were used to estimate the maximum statistical inefficiency $g \equiv 1 + 2 \max(\tau_\rho, \tau_{U_c})$ for each simulation,[64] where $\tau_A \equiv \int_0^\infty C_A(t)dt$ is the mean correlation time for property A computed from the normalized auto-correlation function $C_A(t) = (\langle A(t)A(0)\rangle - \langle A\rangle^2)/(\langle A^2\rangle - \langle A\rangle^2)$. A set of statistically uncorrelated values of ρ was then generated by resampling the time series data using an interval equal to g. Resampled data from simulations performed at the same thermodynamic conditions were combined and reweighted using the multi-state Bennett acceptance ratio[64] (MBAR) method to estimate $F(\rho)$.

At the highest temperature where $F(\rho)$ was calculated (3600 K), a production phase of 150 ns was sufficient to generate ~10^3 independent samples from each simulation. By contrast, production phases of more than 300 ns were required to collect ~10^2 uncorrelated samples in the low-density region at the lowest temperature studied (3000 K). In each case, simulations were equilibrated for more than $50 \times g$ before beginning the production phase. This sampling procedure was sufficient to ensure that statistical uncertainties in $F(\rho)$ from the MBAR estimator were less than $k_B T$ at all of the conditions examined. Unbiased histograms of ρ from adjacent umbrella sampling windows were inspected for hysteresis in regions of overlap to ensure that sampling was performed reversibly. The Steinhardt-Nelson-Ronchetti[65] bond-orientational order parameter Q_6 was also monitored in all simulations to ensure that crystallization did not occur.

III. RESULTS AND DISCUSSION

Equation of state calculations in Ref. 56 show that the magnitude of the Coulombic scaling factor f in Eq. (1) has a profound effect on the apparent phase behavior of the mWAC model. The original model ($f = 1$) exhibits water-like density anomalies and increasing maxima in thermodynamic response functions such as κ_T and C_p upon cooling, but the onset of glassy dynamics prevents scrutiny of its reversible phase behavior at low temperatures where an LLPT may occur. Larger values of f (e.g., 1.08) appear to increase the entropy of LDL-HDL mixing,[56] which prevents an LLPT by causing the system to remain homogeneous at all T. By contrast,

when $f = 0.74$, the predicted LLCP lies below the liquid-vapor spinodal, and cavitation prevents observation of the LLPT.

Here, we investigate the phase behavior of the mWAC model with $f = 0.84$. The equation of state for this variant suggests that it exhibits a fully exposed LLPT in the computationally accessible region of its phase diagram (Fig. 1). The approximate locations of the LLCP and two-phase region are identified by examining the behavior of the isochores (loci of constant ρ) in the $P - T$ plane. In the thermodynamic limit, points where $(\partial P / \partial \rho)_T = 0$ lie along spinodals. These limits of stability bound the two-phase region and terminate upon intersection at the critical point where $(\partial P / \partial \rho)_T = (\partial^2 P / \partial \rho^2)_T = 0$. Points at which the isochores cross satisfy the constraint $(\partial P / \partial \rho)_T = 0$ and therefore signify the location of a spinodal or critical point.

Although this analysis is only strictly valid in the thermodynamic limit, it has been successfully applied to estimate the conditions under which phenomenological behavior consistent with an underlying phase transition may be observed in simulations of finite systems. For the modified WAC model, the isochores begin to converge at low temperatures and eventually cross when $T \lesssim 3500$ K (Fig. 1). Following Ref. 34, estimates of the LLCP, HDL, and LDL spinodals, and temperature of maximum density are obtained by numerically differentiating fits to the simulation data to identify points where the appropriate constraints are satisfied. This procedure yields $T_C = 3350 \pm 75$ K, $P_C = 0.19 \pm 0.09$ GPa, and $\rho_C = 1.8 \pm 0.1$ g cm^{-3} as the approximate location of the LLCP.
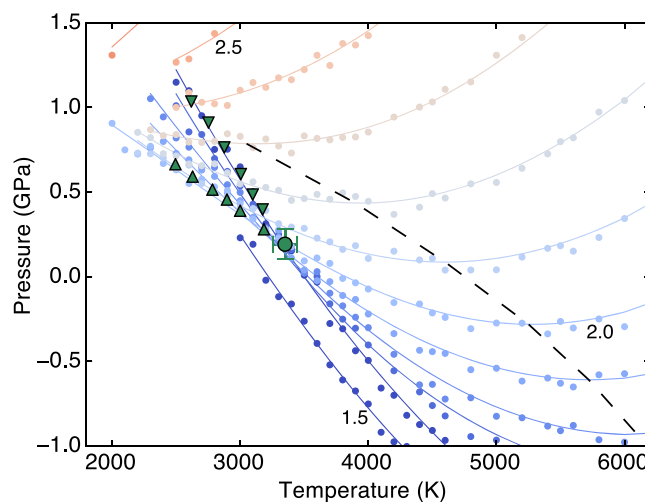

FIG. 1. Equation of state for the mWAC model with $f = 0.84$. Points are data from Ref. 56 that were generated by performing canonical (NVT) ensemble MD simulations of $N = 1500$ particles along isochores (loci of constant density) ranging from 1.5 to 2.6 g cm^{-3}. The isochores are spaced 0.1 g cm^{-3} apart, and select curves corresponding to densities of 1.5, 2.0, and 2.5 g cm^{-3} are marked with numbers. Lines are polynomial fits to the isochore data. Locations where the isochores cross satisfy the constraint $(\partial P / \partial \rho)_T = 0$, which would signify the location of a spinodal or critical point in the thermodynamic limit. In this study, these points are used as finite size estimates of the HDL and LDL spinodals (inverted and regular triangles, respectively) and the LLCP (large circle), which is located approximately at $T_C = 3350 \pm 75$ K, $P_C = 0.19 \pm 0.09$ GPa, and $\rho_C = 1.8 \pm 0.1$ g cm^{-3}. Below the temperature of maximum density (dashed line), the system's density exhibits anomalous behavior and decreases with T.

According to the LLCP hypothesis, thermodynamic response functions, such as κ_T and C_P, should exhibit maxima above the critical point that diverge as $T \rightarrow T_C$. The lines of maxima for κ_T and C_P occur near the Widom line,[4,66] which is defined as the locus of correlation-length maxima in the $P - T$ plane, and all converge at the critical point. Finite size effects in simulation prevent observation of critical singularities and divergence of κ_T and C_P maxima. The response function analysis in Ref. 56 shows, however, that maxima in κ_T and C_P approximately converge for the mWAC model near the estimated location of the LLCP. Similar behavior has been observed in molecular models of water in the vicinity of their predicted LLCPs.

Phenomenological evidence from equation of state calculations suggests that the mWAC model with $f = 0.84$ exhibits an LLPT below $T_C \approx 3350$ K. Accordingly, signatures of two liquids should be observed in free energy calculations performed at $T < T_C$. At a given T, relative phase stabilities are determined by the pressure, which dictates the curvature of the free energy $F(\rho; P, T)$. For pressures that fall within the predicted two-phase region, $F(\rho; P, T)$ should exhibit a double-minimum structure. At coexistence, the phases will be observed with equal probability such that $\int_A \mathcal{P}(\rho; P, T) \, d\rho = \int_B \mathcal{P}(\rho; P, T) \, d\rho$, or equivalently $\int_A e^{-\beta F(\rho; P, T)} \, d\rho = \int_B e^{-\beta F(\rho; P, T)} \, d\rho$, where A and B denote the range of ρ relevant to the free energy basin of each phase, respectively. If the basins have similar shapes, the above equality will be approximately satisfied when the minima are equal. To compute $F(\rho; P, T)$, we perform umbrella sampling in the isothermal–isobaric ensemble at (T, P). Points of approximate coexistence are subsequently located by reweighting using

$$F(\rho; P + \Delta P, T) = F(\rho; P, T) + \Delta PN/\rho \qquad (4)$$

to find conditions $(T, P + \Delta P)$, where the free energy minima have equal depths.

The free energy $F(\rho)$ was computed for $N = 1500$ particles at five temperatures ranging from 3000 to 3600 K [Fig. 2(a)].[67] At 3600 K, $F(\rho)$ exhibits a single, narrow basin at all pressures examined, indicating that only one liquid is present. As T is lowered to 3450 K, the basin widens and its curvature flattens, signifying an increase in the liquid's compressibility. At $T = 3300$ K, $F(\rho)$ exhibits weak bimodal behavior. Upon reweighting in pressure, we observe two basins of equal depth located at $\rho \approx 1.55$ and 2.10 g cm^{-3}, which correspond to LDL and HDL, respectively. The ca. 1 $k_B T$ barrier separating the basins arises from the small, but finite free energy penalty that must be overcome to form an interface between the liquids. Hence the free energy calculations suggest that T_C lies between 3300 and 3450 K, which is consistent with the value of $T_C \approx 3350$ K estimated from the equation of state analysis. Points near HDL–LDL coexistence are also identified at 3150 K and 3000 K. Larger free energy barriers at these conditions (ca. 3.8 and 6.5 $k_B T$, respectively) reflect the increase in L–L surface tension as T decreases further below T_C.

Free energy calculations for mWAC show clear evidence of L–L coexistence inside the two-phase region identified from the model's equation of state. Limits of phase stability can also be estimated by reweighting $F(\rho)$. At
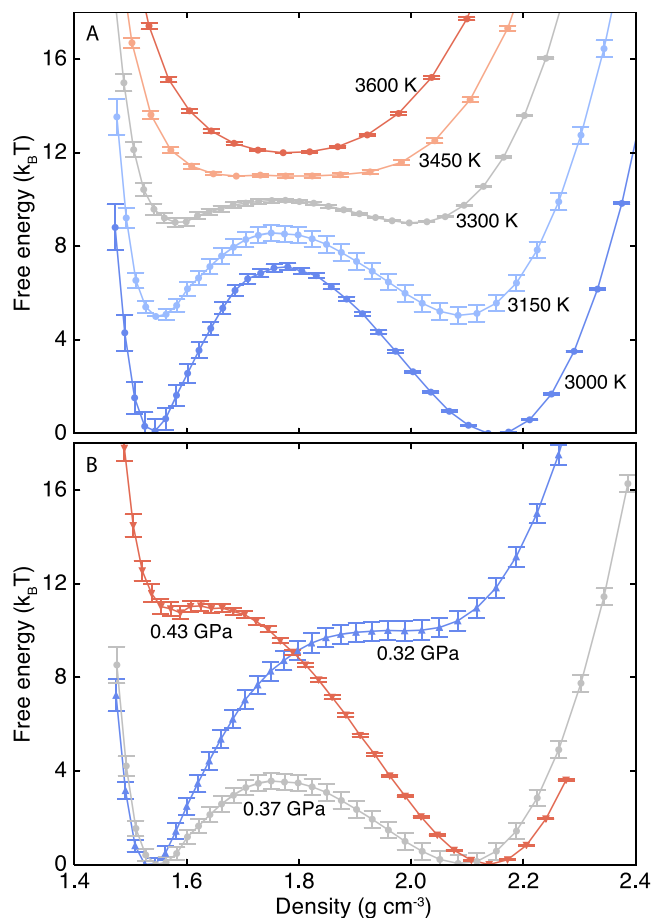

FIG. 2. Free energy $F(\rho)$ for the mWAC model with $f = 0.84$ computed for $N = 1500$ particles. (a) $F(\rho)$ calculated at (3600 K, −0.02 GPa), (3450 K, 0.11 GPa), (3300 K, 0.24 GPa), (3150 K, 0.37 GPa), and (3000 K, 0.50 GPa) by reweighting in pressure. Only a single liquid basin is observed at 3600 and 3450 K. At lower temperatures, $F(\rho)$ exhibits a double-minimum structure; the two basins correspond to HDL ($\rho \approx 2.10$ g cm^{-3}) and LDL ($\rho \approx 1.55$ g cm^{-3}), respectively. (b) Pressure dependence of $F(\rho)$ at 3150 K. The system is near HDL–LDL coexistence at 0.37 GPa. Limits of stability for HDL and LDL are found by reweighting to 0.32 and 0.43 GPa, respectively.

$T = 3150$ K, for example, L–L coexistence occurs near 0.37 GPa [Fig. 2(b)]. Upon compression, LDL loses stability with respect to HDL, until it becomes unstable at 0.43 GPa. Similarly, HDL becomes unstable upon expansion to 0.32 GPa. This marked sensitivity to pressure is consistent with the increased compressibility expected in the vicinity of the LLCP.

The small free energy barriers in $F(\rho)$ near T_C suggest that thermal fluctuations under these conditions should be sufficient to drive the system back and forth between the HDL and LDL basins on the time scales accessible with MD. Indeed, this "phase flipping" behavior has been observed in Ref. 56 in MD simulations performed at 3240 K and 0.30 GPa. Free energy calculations show that this point is near HDL–LDL coexistence and that the barrier separating the liquids is approximately 2 $k_B T$ [Fig. 3(a)]. We study the HDL–LDL transition by initializing 30 unbiased MD simulations in each of the liquid basins at a nearby condition (3240 K and 0.29 GPa). As expected, the MD simulations repeatedly transition between basins over the course of the 200 ns trajectories [Fig. 3(b)]. Because the simulations explore
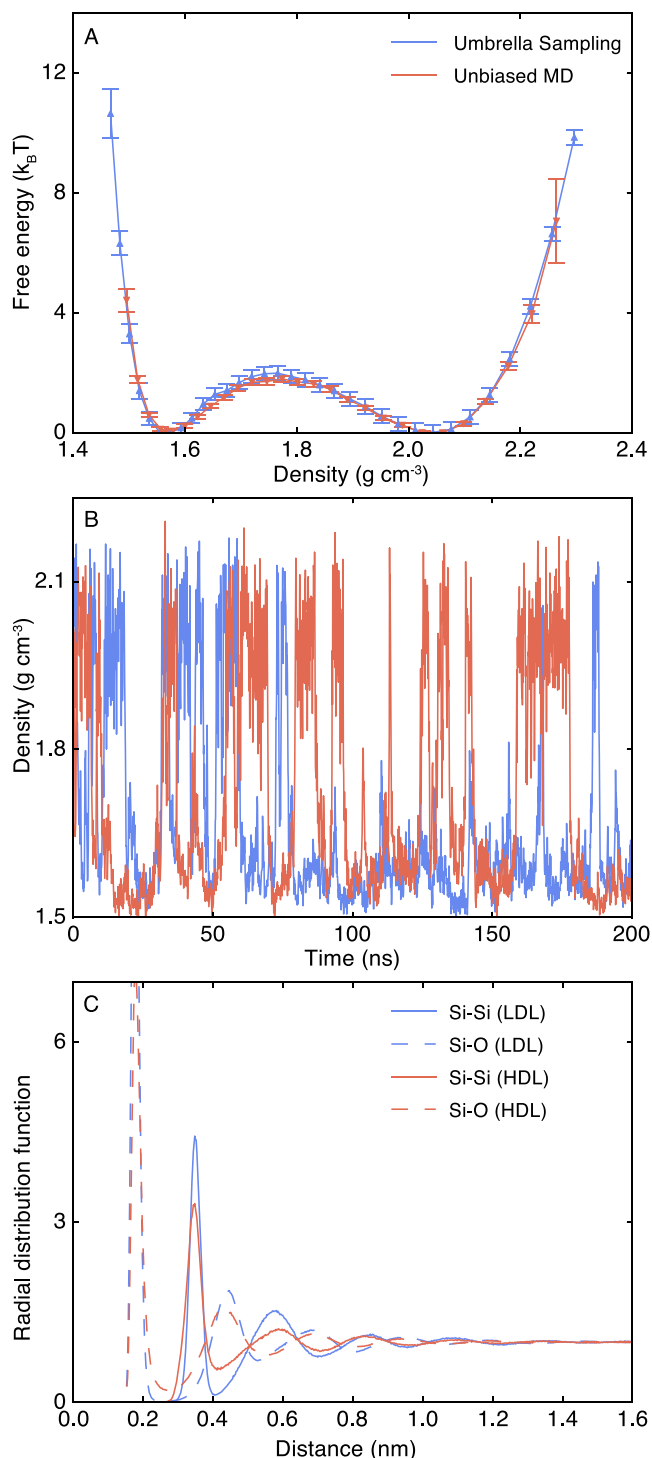
FIG. 3. (a) Free energy $F(\rho)$ for the mWAC model with $f = 0.84$ computed at 3240 K and 0.29 GPa for $N = 1500$ particles using umbrella sampling (blue line) and 60 unbiased MD simulations (red line). (b) Two example trajectories from the unbiased MD simulations, which illustrate "phase flipping" between the HDL and LDL at 3240 K and 0.29 GPa. (c) Radial distribution functions (RDFs) for HDL ($\rho \approx 2.10$ g cm^{-3}) and LDL ($\rho \approx 1.15$ g cm^{-3}) computed using $N = 4500$ particles. LDL is characterized by a tetrahedral coordination structure in which each Si has 4 Si and 4 O nearest neighbors. By contrast, Si is coordinated with 6 Si and 4.5 O^{-2} on average in HDL. Coloring schemes for the three panels are independent.

the full range of density fluctuations relevant to the LLPT, $F(\rho)$ can be estimated directly using uncorrelated samples of ρ obtained from the time series data produced by the MD

trajectories. The resulting estimate of $F(\rho)$ is in excellent agreement with the free energy computed using umbrella sampling [Fig. 3(a)].

We emphasize that the LLPT in the mWAC model is not driven by a demixing into two phases of different densities and different compositions, as might happen in simple binary mixtures. The HDL–LDL transition occurs in simulated systems where the ion composition is fixed such that Si^{+4} and O^{-2} always appear in an electrically neutral 1:2 ratio. This fact is illustrated by the unbiased MD trajectories, in which "phase flipping" is observed. Instead, the LDL and HDL phases differ in density and structure. Radial distribution functions (RDFs) computed for the two phases show that LDL has greater short-range order and more pronounced Si–Si and Si–O first and second neighbor peaks [Fig. 3(c)]. Integration over the first peak of the RDFs reveals that LDL has a tetrahedral coordination structure in which Si is coordinated with 4 Si and 4 O nearest neighbors on average. By contrast, each Si has ca. 6 Si and 4.5 O nearest neighbors on average in HDL. Similar coordination structures are also observed in molecular models of water such as ST2. Whereas ST2's LDL phase is tetrahedrally ordered, its HDL is characterized by the addition of a fifth molecule into the interstitial region between the first and second coordination shells. Hence, in both ST2 and mWAC, tetrahedral order is partially disrupted in the HDL phase by the intrusion of additional neighbors into the first coordination shell.

The free energy barriers observed in $F(\rho)$ reflect the energy penalty to form an L–L interface. For the small systems used to compute $F(\rho)$, the interface cannot be clearly identified because it manifests itself through the formation of clusters with local environment characteristic of each distinct liquid phase. In principle, a stable L–L interface should be observed, however, upon quenching a large system of constant density into the two-phase region, where HDL and LDL are immiscible.[68] To examine this behavior, we performed large-scale MD simulations in the canonical (NVT) ensemble using $N = 108\,000$ particles. The simulations were equilibrated at an initial high temperature (5000 K) for 1 ns. The set point of the thermostat was then lowered instantaneously to quench the system to its final temperature. Each trajectory was propagated for 100 ns following the quench to observe the system's response.

Depending on the simulation cell geometry, the immiscible liquids will form spherical, cylindrical, or planar interfaces to minimize the system's free energy.[68] To promote formation of planar interfaces, which are easiest to observe and characterize, we use a rectangular box with an aspect ratio of $L_x:L_y:L_z = 1:1:3$. Assuming the L–L surface tension γ_{L-L} is independent of the cell geometry, one can show that this cell aspect ratio will favor formation of two planar interfaces perpendicular to the z-direction if the minority phase occupies more than ca. 11% of the cell volume.[68] This condition is easily satisfied by using the lever rule to find an appropriate choice for the system density, which will fall in between the values expected for the HDL and LDL phases. We chose 1.87 g cm^{-3}, which corresponds to cell dimensions of $L_x = L_y = 8.616$ nm and $L_z = 25.849$ nm, for the selected system size.
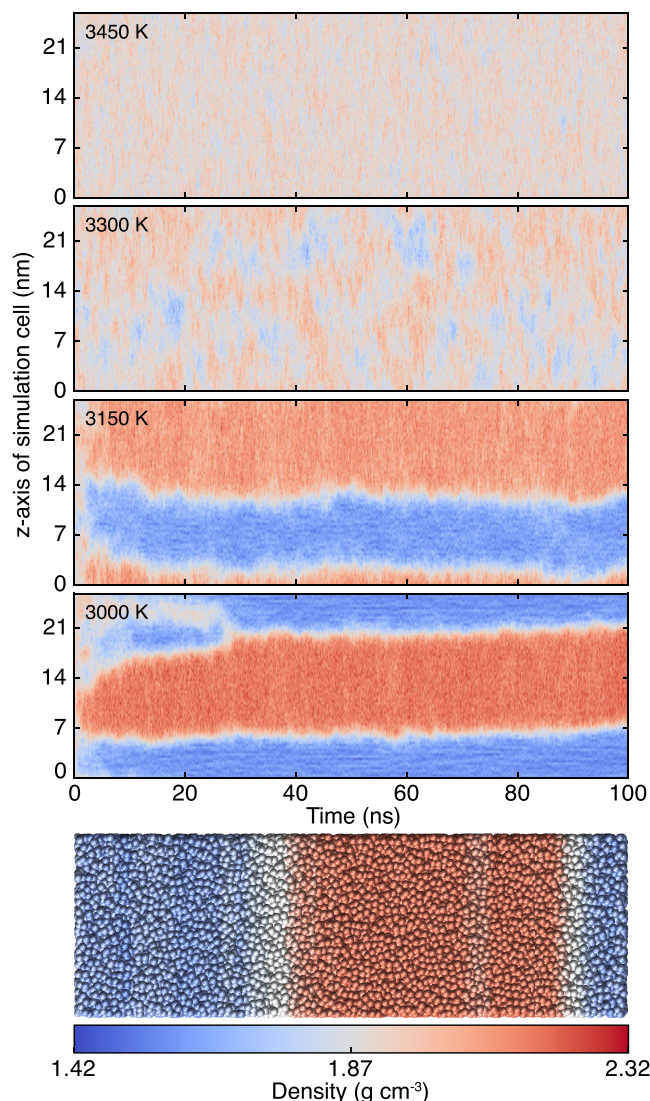
FIG. 4. (top) Evolution of the density profile in MD simulations of N = 108 000 particles after quenching from 5000 K to the final temperature denoted in each panel at $t = 0$. The density profiles are computed along the z-axis of the rectangular simulation cell (L_z = 25.849 nm), which has an aspect ratio of $L_x{:}L_y{:}L_z$ = 1:1:3. The mean density is fixed at 1.87 g cm^{-3}, which is in between the characteristic values for HDL and LDL. At 3150 and 3000 K ($T < T_C$), the system phase separates into large domains of HDL and LDL. The HDL and LDL regions are separated by planar interfaces approximately 74.2 nm^2 in size, which span the x- and y-dimensions of the cell. (bottom) The HDL–LDL interfaces are observed in renderings of the system at 3000 K in which the particles are shaded according to the local density across the z-axis of the simulation cell.

The formation of an L–L interface was monitored by dividing the system into 80 equal slabs (1 every ca. 0.32 nm) along the z-direction of the simulation cell and tracking the density in each slab as a function of time, following the quench at $t = 0$ (Fig. 4). For T = 3450 K, the system remains homogeneous over the entire MD trajectory and no signs of an L–L interface are observed. This behavior is consistent with the equation of state and free energy calculations (Figs. 1 and 2, respectively), which predict that only a single liquid phase is stable above $T_C \approx 3350$ K. At 3300 K, small high-density and low-density domains are observed, but complete phase separation does not occur. Although $T \lesssim T_C$ under these conditions, large critical density fluctuations in the vicinity

of T_C prevent complete phase separation and formation of a stable interface. Similar behavior has been noted in simulations performed for water models and Lennard-Jones fluids slightly below their respective vapor-liquid critical points.[68,69] Alternatively, the actual location of the LLCP could lie below the estimated value of 3350 K. The small barrier observed in $F(\rho)$ at 3300 K may therefore be due to finite size artifacts, which are inevitable in simulations performed near critical conditions.

As the temperature is lowered and γ_{L-L} increases, the HDL- and LDL-like domains grow until they span large sections of the simulation cell. At 3150 and 3000 K, spontaneous phase separation occurs, demonstrating that HDL and LDL are immiscible under these conditions (Fig. 4). The phase separation process occurs rapidly because inter-conversion between HDL and LDL only requires small rearrangements in the atomic coordination structure. Indeed, for purely density-driven transitions, the equilibration time scale is set by the propagation velocity of momentum (sound) waves, which travel quickly through liquids. By contrast, much slower diffusion time scales control equilibration in transitions that involve phases of different compositions. The L–L interfaces that form following the quench are observed clearly in renderings of the systems in which the particles are shaded according to the local density inside the bin where they reside (Fig. 4). Hence, in accord with equation of state and free energy calculations, the large-scale MD simulations show that a clear density-driven LLPT occurs in the mWAC model below $T_C \approx 3350$ K.

IV. CONCLUSIONS

The WAC model of silica exhibits water-like thermo-physical anomalies but no signs of an LLPT in the computationally accessible region of its phase diagram. Recent equation of state calculations suggest, however, that a fully exposed LLPT occurs in a modified WAC (mWAC) model, in which the strength of the Coulombic interaction is reduced to enhance tetrahedral order in the liquid.[56] Here, we performed extensive umbrella sampling free energy calculations to rigorously scrutinize the low-temperature phase behavior of the mWAC model. Below the estimated critical temperature $T_C \approx 3350$ K, we find two distinct liquid basins in the free energy $F(\rho)$, which correspond to HDL and LDL, respectively. By reweighting $F(\rho)$ in pressure, we identified points of HDL–LDL coexistence and the stability limits of the liquids.

We also performed unbiased MD simulations to study the LLPT in the mWAC model. Constant pressure MD simulations conducted near L–L coexistence with N = 1500 particles repeatedly exhibit abrupt transitions between the HDL and LDL. The estimate of $F(\rho)$ computed from these "phase flipping" trajectories exhibits two liquid basins and is in excellent quantitative agreement with rigorous umbrella sampling calculations. The LLPT in mWAC was also observed directly in large constant density MD simulations of N = 108 000 particles. Upon quenching these systems into the two-phase region, we observed the formation of large HDL and LDL domains that spanned the simulation cell. The use of

a long, rectangular simulation cell promoted the formation of sharp planar interfaces between the HDL and LDL domains, which were observed directly in the MD trajectories.

Our investigation shows that the mWAC model of silica exhibits an unmistakable LLPT at low temperatures. This transition occurs between two liquids that have identical compositions but different densities. The LDL phase is characterized by strong tetrahedral order, which is partially disrupted in HDL by intrusion of additional neighbors into the primary coordination shells of the Si and O ions. In this regard, the LLPT in mWAC is consistent with the LLCP hypothesis that has been invoked to explain the thermodynamic anomalies of water and other tetrahedral liquids. With the exception of the ST2 model of water,[42,43] however, slow structural relaxations have prevented confirmation of the existence of such a transition in other atomistic tetrahedral liquid models. By contrast, we find that equilibration of the mWAC model is facile, requiring less than ca. 5 ns to relax the systems at all conditions examined in the present study. Hence, we anticipate that the computational convenience of the mWAC model will facilitate future studies aimed at understanding low-temperature, density-driven LLPTs and their connection with the anomalous thermodynamic behaviors exhibited by tetrahedral liquids.

ACKNOWLEDGMENTS

[1] P. Ball, *Life's Matrix: A Biography of Water*, 1st ed. (Farrar, Straus, and Giroux, New York, 2000), p. xvi, p. 417.
[2] F. Franks, *Water: A Matrix of Life*, RSC Paperbacks, Royal Society of Chemistry (Great Britain), 2nd ed. (Royal Society of Chemistry, Cambridge, UK, 2000), p. xii, p. 225.
[3] P. G. Debenedetti, J. Phys.: Condens. Matter **15**, R1669 (2003).
[4] P. Gallo, K. Arnann-Winkel, C. A. Angell, M. A. Anisimov, F. Caupin, C. Chakravarty, E. Lascaris, T. Loerting, A. Z. Panagiotopoulos, J. Russo, J. A. Sellberg, H. E. Stanley, H. Tanaka, C. Vega, L. M. Xu, and L. G. M. Pettersson, Chem. Rev. **116**, 7463 (2016).
[5] C. A. Angell, J. Shuppert, and J. C. Tucker, J. Phys. Chem. **77**, 3092 (1973).
[6] R. J. Speedy and C. A. Angell, J. Chem. Phys. **65**, 851 (1976).
[7] H. Kanno and C. A. Angell, J. Chem. Phys. **70**, 4008 (1979).
[8] C. A. Angell, M. Oguni, and W. J. Sichina, J. Phys. Chem. **86**, 998 (1982).
[9] M. Oguni and C. A. Angell, J. Chem. Phys. **78**, 7334 (1983).
[10] B. J. Mason, Adv. Phys. **7**, 221 (1958).
[11] R. J. Speedy, J. Phys. Chem. **86**, 982 (1982).
[12] P. H. Poole, F. Sciortino, U. Essmann, and H. E. Stanley, Nature **360**, 324 (1992).
[13] S. Sastry, P. G. Debenedetti, F. Sciortino, and H. E. Stanley, Phys. Rev. E **53**, 6144 (1996).
[14] C. A. Angell, Science **319**, 582 (2008).
[15] D. T. Limmer and D. Chandler, J. Chem. Phys. **135**, 134503 (2011).
[16] O. Mishima, L. D. Calvert, and E. Whalley, Nature **314**, 76 (1985).
[17] K. Amann-Winkel, C. Gainaru, P. H. Handle, M. Seidl, H. Nelson, R. Bohmer, and T. Loerting, Proc. Natl. Acad. Sci. U. S. A. **110**, 17720 (2013).
[18] K. Amann-Winkel, R. Bohmer, F. Fujara, C. Gainaru, B. Geil, and T. Loerting, Rev. Mod. Phys. **88**, 011002 (2016).
[19] J. A. Sellberg, C. Huang, T. A. McQueen, N. D. Loh, H. Laksmono, D. Schlesinger, R. G. Sierra, D. Nordlund, C. Y. Hampton, D. Starodub, D. P. DePonte, M. Beye, C. Chen, A. V. Martin, A. Barty, K. T. Wikfeldt, T. M. Weiss, C. Caronna, J. Feldkamp, L. B. Skinner, M. M. Seibert, M. Messerschmidt, G. J. Williams, S. Boutet, L. G. M. Pettersson, M. J. Bogan, and A. Nilsson, Nature **510**, 381 (2014).
[20] H. Pathak, J. C. Palmer, D. Schlesinger, K. T. Wikfeldt, J. A. Sellberg, L. G. M. Pettersson, and A. Nilsson, J. Chem. Phys. **145**, 134507 (2016).
[21] A. Haji-Akbari and P. G. Debenedetti, Proc. Natl. Acad. Sci. U. S. A. **112**, 10582 (2015).
[22] J. C. Palmer and P. G. Debenedetti, AIChE J. **61**, 370 (2015).
[23] G. C. Sosso, J. Chen, S. J. Cox, M. Fitzner, P. Pedevilla, A. Zen, and A. Michaelides, Chem. Rev. **116**, 7078 (2016).
[24] V. Molinero and E. B. Moore, J. Phys. Chem. B **113**, 4008 (2009).
[25] E. B. Moore and V. Molinero, Nature **479**, 506 (2011).
[26] J. C. Palmer, R. S. Singh, R. J. Chen, F. Martelli, and P. G. Debenedetti, Mol. Phys. **114**, 2580 (2016).
[27] J. L. F. Abascal and C. Vega, J. Chem. Phys. **133**, 234502 (2010).
[28] R. S. Singh, J. W. Biddle, P. G. Debenedetti, and M. A. Anisimov, J. Chem. Phys. **144**, 144504 (2016).
[29] D. Paschek, Phys. Rev. Lett. **94**, 217802 (2005).
[30] J. Russo and H. Tanaka, Nat. Commun. **5**, 3556 (2014).
[31] Y. P. Li, J. C. Li, and F. Wang, Proc. Natl. Acad. Sci. U. S. A. **110**, 12209 (2013).
[32] Y. C. Ni and J. L. Skinner, J. Chem. Phys. **144**, 214501 (2016).
[33] F. H. Stillinger and A. Rahman, J. Chem. Phys. **60**, 1545 (1974).
[34] P. H. Poole, I. Saika-Voivod, and F. Sciortino, J. Phys.: Condens. Matter **17**, L431 (2005).
[35] M. J. Cuthbertson and P. H. Poole, Phys. Rev. Lett. **106**, 115706 (2011).
[36] V. Holten, J. C. Palmer, P. H. Poole, P. G. Debenedetti, and M. A. Anisimov, J. Chem. Phys. **140**, 104502 (2014).
[37] Y. Liu, A. Z. Panagiotopoulos, and P. G. Debenedetti, J. Chem. Phys. **131**, 104508 (2009).
[38] F. Sciortino, I. Saika-Voivod, and P. H. Poole, Phys. Chem. Chem. Phys. **13**, 19759 (2011).
[39] Y. Liu, J. C. Palmer, A. Z. Panagiotopoulos, and P. G. Debenedetti, J. Chem. Phys. **137**, 214505 (2012).
[40] P. H. Poole, R. K. Bowles, I. Saika-Voivod, and F. Sciortino, J. Chem. Phys. **138**, 034505 (2013).
[41] J. C. Palmer, R. Car, and P. G. Debenedetti, Faraday Discuss. **167**, 77 (2013).
[42] J. C. Palmer, F. Martelli, Y. Liu, R. Car, A. Z. Panagiotopoulos, and P. G. Debenedetti, Nature **510**, 385 (2014).
[43] F. Smallenburg and F. Sciortino, Phys. Rev. Lett. **115**, 015701 (2015).
[44] F. W. Starr and F. Sciortino, Soft Matter **10**, 9413 (2014).
[45] F. Smallenburg, L. Filion, and F. Sciortino, Nat. Phys. **10**, 653 (2014).
[46] F. H. Stillinger and T. A. Weber, Phys. Rev. B **31**, 5262 (1985).
[47] S. Sastry and C. Austen Angell, Nat. Mater. **2**, 739 (2003).
[48] D. T. Limmer and D. Chandler, J. Chem. Phys. **138**, 214504 (2013).
[49] F. Ricci, J. C. Palmer, and P. G. Debenedetti, "A computational investigation of the thermodynamics of the Stillinger-Weber family of models at supercooled conditions" (unpublished).
[50] P. H. Poole, M. Hemmati, and C. A. Angell, Phys. Rev. Lett. **79**, 2281 (1997).
[51] I. Saika-Voivod, F. Sciortino, and P. H. Poole, Phys. Rev. E **63**, 011202 (2000).
[52] B. W. H. van Beest, G. J. Kramer, and R. A. van Santen, Phys. Rev. Lett. **64**, 1955 (1990).
[53] L. V. Woodcock, C. A. Angell, and P. Cheeseman, J. Chem. Phys. **65**, 1565 (1976).
[54] M. S. Shell, P. G. Debenedetti, and A. Z. Panagiotopoulos, Phys. Rev. E **66**, 011202 (2002).
[55] E. Lascaris, M. Hemmati, S. V. Buldyrev, H. E. Stanley, and C. A. Angell, J. Chem. Phys. **140**, 224502 (2014).
[56] E. Lascaris, Phys. Rev. Lett. **116**, 125701 (2016).
[57] T. A. Kesselring, E. Lascaris, G. Franzese, S. V. Buldyrev, H. J. Herrmann, and H. E. Stanley, J. Chem. Phys. **138**, 244506 (2013).
[58] G. Torrie and J. Valleau, J. Comput. Phys. **23**, 187 (1977).
[59] S. Pronk, S. Pll, R. Schulz, P. Larsson, P. Bjelkmar, R. Apostolov, M. R. Shirts, J. C. Smith, P. M. Kasson, D. van der Spoel, B. Hess, and E. Lindahl, Bioinformatics **29**, 845 (2013).
[60] S. Nosé, Mol. Phys. **52**, 255 (1984).
[61] W. G. Hoover, Phys. Rev. A **31**, 1695 (1985).
[62] M. Parrinello and A. Rahman, J. Appl. Phys. **52**, 7182 (1981).
[63] G. A. Tribello, M. Bonomi, D. Branduardi, C. Camilloni, and G. Bussi, Comput. Phys. Commun. **185**, 604 (2014).
[64] M. R. Shirts and J. D. Chodera, J. Chem. Phys. **129**, 124105 (2008).

[65] P. J. Steinhardt, D. R. Nelson, and M. Ronchetti, Phys. Rev. B **28**, 784 (1983).

[66] L. Xu, P. Kumar, S. V. Buldyrev, S.-H. Chen, P. H. Poole, F. Sciortino, and H. E. Stanley, Proc. Natl. Acad. Sci. U. S. A. **102**, 16558 (2005).

[67] Molecular dynamics simulations were performed at (3600 K, 0.05 GPa), (3450 K, 0.10 GPa), (3300 K, 0.23 GPa), (3150 K, 0.35 GPa), and (3000 K, 0.49 GPa). The free energy profiles shown in Fig. 2(a) were obtained by reweighting from these conditions.

[68] T. Yagasaki, M. Matsumoto, and H. Tanaka, Phys. Rev. E **89**, 020301 (2014).

[69] J. T. Fern, D. J. Keffer, and W. V. Steele, J. Phys. Chem. B **111**, 13278 (2007).